Soil Dynamics and Earthquake Engineering 101 (2017) 269–284

Contents lists available at ScienceDirect

Soil Dynamics and Earthquake Engineering

journal homepage: www.elsevier.com/locate/soildyn

Dynamic behavior of fiber-reinforced soil under freeze-thaw cycles

Muge Elif Orakoglu[a,b], Jiankun Liu[a,*], Fujun Niu[c]

[a] School of Civil Engineering, Beijing Jiaotong University, Beijing 100044, China
[b] Technical Education Faculty, Construction Department, Firat University, Elazig 23000, Turkey
[c] State Key Laboratory of Frozen Soil Engineering, Cold and Arid Regions Environmental and Engineering Research Institute, Chinese Academy of Sciences, Lanzhou 730000, China

ARTICLE INFO

Keywords:
Fiber-reinforced soil
Dynamic test parameters
Freeze-thaw cycles
Theoretical analytical formulations

ABSTRACT

This research presents the dynamic behavior of fiber-reinforced soil exposed to freeze-thaw cycles. The series of dynamic triaxial tests were conducted on fine-grained soil mixed with different percentages of basalt and glass fibers subjected to freeze-thaw cycles. The results showed that after freeze-thaw cycles, with the addition of basalt and glass fibers, the damping ratio and the shear modulus increased at a constant confining pressure because of the increase of stiffness, but the shear modulus decreased with increasing shear strain. Moreover, the theoretical analytical formulations were developed to define for dynamic shear stress and dynamic shear modulus. The parameters were predicted by Hardin-Drnevich model and Kondner-Zelasko model. The shear modulus was expressed as a function of freeze-thaw cycles, fiber contents, confining pressure and initial water content. Finally, ten coefficients were calibrated by analyzing the experimental results and then employed to describe dynamic shear modulus of the fiber-reinforced soil.

1. Introduction

The dynamic properties of material used in geotechnical engineering were greatly influenced by dynamic shear modulus and damping ratio. In soil dynamic problems, stress-strain behavior of soil is always expressed by Hysteresis loops where the shear resistance and damping ratio is defined as the slope of lines related to top point of loops and the areas enveloped by loops, respectively. Many dynamic problems including earthquake incidence, machine vibrations, and ocean waves can be solved by the determination of energy absorption and stiffness of soil-structure interaction. Moreover, recent researches on geotechnical engineering technology indicated that soil reinforcement improves the resistance of soil against compression and tension. In terms of the wide use of soil reinforcement in geotechnical engineering, the potential benefit of soil reinforcement under dynamic loading should be investigated. In the literature, many experimental and numerical researches have been focused on the reinforced soil with different types of fiber. These results showed that the tensile strength of soil can be improved obviously with the fibers [1–7]. On the other hand, recent studies on liquefaction potential of fiber-reinforced soil have shown that the liquefaction of retaining structures, embankments and subgrade soil was influenced by fiber content, fiber length and number of loading cycles [8–14].

Dynamic characteristics of reinforced soils are greatly influenced by many parameters such as fiber content, fiber length, freeze-thaw cycles, loading repetition, confining pressure, frequency and shear strain amplitude. Shahnazari et al. [15] investigated the dynamic effects of reinforced sand with carpet and geotextile strips by conducting large and small scale of cyclic triaxial tests. The results showed that the shear modulus of reinforced soils decreased in the low confining pressures (less than 100 kPa) and increased in the high confining pressures [15]. Naeini and Gholampoor (2014) carried out a number of cyclic triaxial tests on reinforced silty sand with geotextile. Their results showed that the dynamic axial modulus increased and the cyclic ductility of silty sand for all silt contents decreased with the increments of number of geotextile layers and confining pressure. Moreover, with the addition of silt up to about 35%, dynamic axial modulus reduced and cyclic ductility increased [16]. Also, Sadeghi and Beigi (2014) conducted a number of triaxial tests to examine the effect of fiber content, deviator stress ratio, confining pressure, and number of loading cycles on secant dynamic shear modulus of fiber-reinforced soil. The results indicated that an increment of deviator stress ratio caused a decrease on the dynamic shear modulus at a high confining pressures. Also, the increment of dynamic shear modulus with loading repetition was expressed at a large deviator stress ratio [17]. Kirar et al. [18] conducted a large number of undrained cyclic triaxial tests on the cylindrical unreinforced and reinforced sand specimens with different percentages of coir fiber. The authors concluded that the effects of fiber content were expressed

* Corresponding author.
E-mail addresses: mugeorakoglu@gmail.com (M. Elif Orakoglu), jkliu@bjtu.edu.cn (J. Liu), niufujun@lzb.ac.cn (F. Niu).

http://dx.doi.org/10.1016/j.soildyn.2017.07.022
Received 8 March 2016; Received in revised form 14 June 2017; Accepted 30 July 2017

Table 1
The particle size distribution and the engineering properties of clay soil.

Grain composition* (%)				Dry density gr/cm^3	Optimum water content (%)	Plasticity index
d > 0.01	0.01 ≥ d ≥ 0.005	0.005 ≥ d > 0.005	d ≤ 0.001	1.80	18.03	8.05
67.29	11.16	15.95	5.59			

* Determined by a laser particle size analyzer Mastersize 2000.
*Classified as CL according to the Unified Soil Classification System.

as a function of stress–strain amplitude and confining stress. It was found that effect of fiber content was significant on both dynamic shear modulus and damping ratio especially at higher shear strain amplitude [18]. Nakhaei et al. [19] carried out large-scale consolidated-undrained cyclic triaxial tests on reinforced soil with granulated rubber and specific granular soil to investigate the effects of reinforcement materials on dynamic shear modulus and damping ratio. Their results showed that the dynamic shear modulus increased with increase of confining pressure and decreased with the increase of the rubber content. Furthermore, the damping ratio decreased with the addition of rubber under low confining pressure (σ_c = 50 kPa and 100 kPa) and increased with increase of rubber content under high confining pressure [19].

Moreover, various models and methods related to failure criteria, plastic theory and limit analysis under dynamic loading were developed by many researchers to investigate the dynamic behavior of reinforced soil [3,20–28]. On the other hand, soil reinforcement with different types of fiber plays a significant role in mechanical and thermal properties of soil. In this study, two different types of fiber including glass fiber and basalt fiber were used to investigate their effects on the dynamic and physical properties. The glass fiber with different blended ratios was often used to investigate the engineering properties of soil. However, this fiber was not studied enough under freeze-thaw cycles in the literature. Further, the glass fiber has the wide use in civil and highway engineering. In this application, the glass fiber presents effective bulk density, hardness, stability, flexibility and stiffness. Besides, the basalt fiber was not studied enough in reinforced soil to improve engineering properties although these fibers are generally used as an alternative to metal reinforcements in building materials, such as steel and aluminum. Moreover, the basalt is used in reinforcement technology to stabilize the pavement by decreasing effects of cracks caused by excessive traffic loading, age hardening and temperature variations. In view of these useful and advantageous properties of basalt and glass fibers, physical properties and dynamic behavior of reinforced soil by all these fibers subjected to freeze-thaw cycles were studied.

The aim of this research was to elucidate the effects of freeze-thaw cycles on physical properties and dynamic behavior of reinforced clayey soils with randomly distributed glass and basalt fibers. For this purpose, dynamic triaxial tests were conducted under different number of freeze-thaw cycles, fiber contents, and confining pressures. The theoretical analytical formulations proposed by Hardin-Drnevich model and Kondner-Zelasko model were used to determine dynamic shear stress and dynamic shear modulus. The dynamic shear modulus, G_d, was expressed as a function of fiber content (χ), confining pressure (σ_c), water content (w) and freeze-thaw cycle (N). Finally, ten constitutive coefficients of the theoretical analytical formulations were calibrated by analyzing the experimental results, which were then employed to define the G_d of the fiber-reinforced soil.

2. Laboratory experiments

2.1. Tested material

In this paper, clay soil from the Qinghai-Tibet Plateau in China was used to study the dynamic behavior. The particle size distribution and engineering properties of the clayey soil are shown in Table 1.

The specimens were reinforced by basalt and glass fibers with the same length and diameter. Further, the specimens were blended with 0%, 0.5% and 1% ratios of fibers. The basalt and glass fibers were derived from Hebei province in China and relevant engineering properties are presented in Table 2.

2.2. Specimen preparation

The size of the columns specimens were 125 mm in height with a diameter 61.8 mm. For every mixture, the exact weight of each additive material was defined based on optimum moisture content and maximum dry density obtained from the standard Proctor test. Dry soil was mixed with water before the fibers were incorporated uniformly and all soil specimens were compacted by three layers.

2.3. Freeze-thaw performance

The freeze-thaw tests were carried out on the two different parts.

Table 2
Mechanical and physical properties of the studied basalt and glass fibers [29].

	Basalt Fiber	Glass Fiber
		
Breaking strength	3900 MPa	3450 MPa
Modulus of elasticity	86.2 GPa	74 GPa
Breaking extension	3.1%	4.7%
Fiber diameter	10 µm	10 µm
Linear density	60–4200 tex	40–4200 tex
Length	15 mm	15 mm

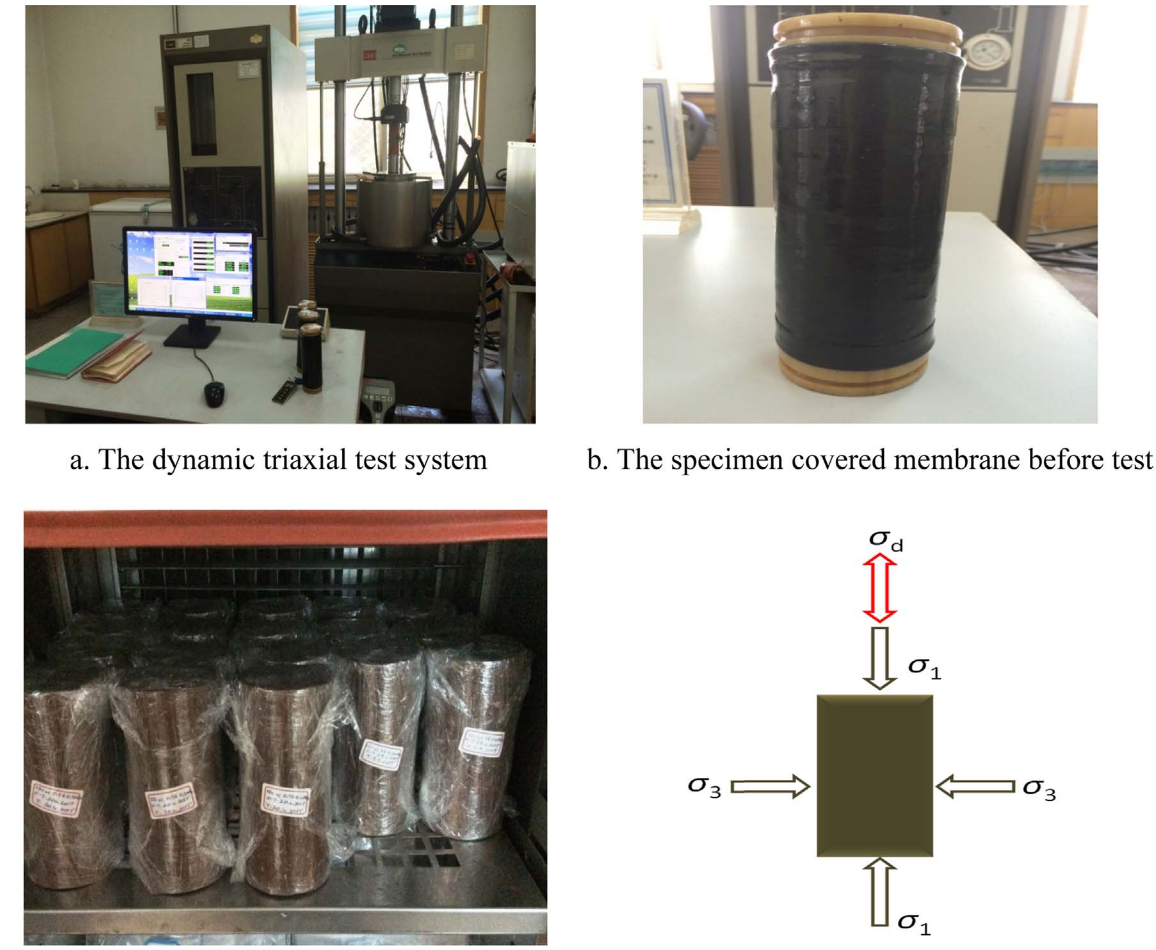

a. The dynamic triaxial test system

b. The specimen covered membrane before test

c. The specimens in the automatic temperature controlled fridge

d. Schematic diagram of specimen subjected to loading

Fig. 1. Dynamic triaxial testing system. a. The dynamic triaxial test system. b. The specimen covered membrane before test. c. The specimens in the automatic temperature controlled fridge. d. Schematic diagram of specimen subjected to loading.

Table 3
Summary of dynamic stress amplitudes (σ_d).

Loading stages	1	2	3	4	5	6	7	8	9	10	…
σ_d (MPa)	0.30	0.60	0.90	1.20	1.50	1.80	2.10	2.40	2.70	3.00	…

Firstly, to determine the effects of freeze-thaw cycles on the physical properties of the fiber-reinforced soil, the specimens were exposed to 0, 2, 5, 10, and 15 freeze-thaw cycles in an open-system. Secondly, to determine the effects of freeze-thaw cycles on the dynamic triaxial behaviors of fiber-reinforced soil, all specimens of dynamic triaxial test were exposed to 0, 2, 5, 10, and 15 freeze-thaw cycles in a close-system and then subjected to dynamic triaxial tests in a closed system. The specimens were exposed to temperature changes in a digital refrigerator for one cycle and the specimen was first frozen at −15 °C for 12 h before thawn at 20 °C for another 12 h. The freezing temperature was chosen with respect to climatic conditions of the studied area and against to the state of incomplete freezing or no freezing due to the absence of ice nucleation. Moreover, Zimmie et al. [30] and Wang et al. [31] showed that the freezing temperature in the experiment should be kept away from near to 0 °C [30,31].

As surface temperature approaches freezing point, the water in soil particles begins to freeze. As a result, the physical parameters including height and water content of soil reformed with emerging ice particles. A certain phenomenon of the freeze-thaw period is the frost heave. The different effects on volumetric changes of the specimen are seen when the soil freezes or thaws. In the freezing process, the height of specimen increases while the height of specimen decreases in the thawing period. Nevertheless, these volume changes in the periods of freezing and thawing are not equal to initial height of the specimen. In this purpose, the height variations of fiber-reinforced specimens after freeze-thaw cycles were evaluated through a dimensionless parameter, H as the following:

$$H = \frac{\Delta H}{H_0} \tag{1a}$$

where ΔH is the difference between the initial height and the height after N cycles in the thawed phase, H_o is the initial height of specimen in the unfrozen soil.

In cold regions, soil particles are formed in various shapes and sizes with binded by a thin layer of unfrozen water film. The water or ice in voids affects permeability, porosity and soil density. A dimensionless parameter, D, for soil specimens after freeze-thaw cycles has been determined to represent the effect of the freezing-thawing cycle on water content of the soil specimen as follows [31]:

Table 4
Summary of testing scheme.

Specimen no	Freeze-thaw cycles, N	Loading frequency, f	Fiber content (%), χ		Confining pressure, (MPa) σ_c
			B	G	
S1	0, 2, 5, 10, 15	1 Hz	0	0	0.3
S2	0, 2, 5, 10, 15	1 Hz	0	0	0.4
S3	0, 2, 5, 10, 15	1 Hz	0	0	0.5
S-0.5G1	0, 2, 5, 10, 15	1 Hz	0	0.5	0.3
S-0.5G2	0, 2, 5, 10, 15	1 Hz	0	0.5	0.4
S-0.5G3	0, 2, 5, 10, 15	1 Hz	0	0.5	0.5
S-1G1	0, 2, 5, 10, 15	1 Hz	0	1	0.3
S-1G2	0, 2, 5, 10, 15	1 Hz	0	1	0.4
S-1G3	0, 2, 5, 10, 15	1 Hz	0	1	0.5
S-0.5B1	0, 2, 5, 10, 15	1 Hz	0.5	0	0.3
S-0.5B2	0, 2, 5, 10, 15	1 Hz	0.5	0	0.4
S-0.5B3	0, 2, 5, 10, 15	1 Hz	0.5	0	0.5
S-1B1	0, 2, 5, 10, 15	1 Hz	1	0	0.3
S-1B2	0, 2, 5, 10, 15	1 Hz	1	0	0.4
S-1B3	0, 2, 5, 10, 15	1 Hz	1	0	0.5

S is soil; S-0.5 G is reinforced soil with 0.5% Glass fiber; S-1 G is reinforced soil with 1% Glass fiber; S-0.5B is reinforced soil with 0.5% Basalt fiber; S-1B is reinforced soil with 1% Basalt fiber; G is glass fiber; B is basalt fiber.

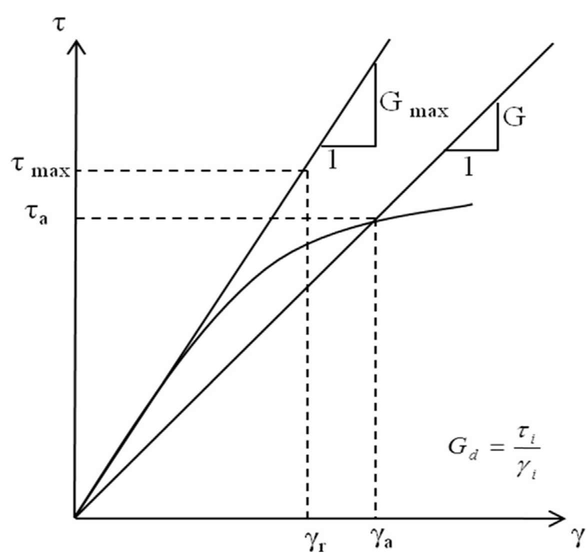

Fig. 2. Determination of G_d and D_i.

$$D = \frac{\Delta w}{w_0} \tag{1b}$$

where Δw is increasing amount of the water content after N cycles in the thawed phase, w_o is the initial water content in the unfrozen soil.

2.4. Apparatus and testing procedure

MTS-810, a dynamic triaxial compression test device, was employed to study the dynamic behavior of fiber-reinforced soil in this study. As depicted in Figs. from 1a to d, the apparatus is capable of both strain-controlled and stress-controlled cyclic loading test which can be performed on the apparatus. The confining pressure ranged from 0 MPa to 20 MPa, the frequency can be changed from 0 Hz to 50 Hz, the maximum axial load was 100 kN, and maximum axial displacement was 85 mm.

The methodology of dynamic triaxial test is simply expressed with a sinusoidal stress (σ_d) applied on a specimen under confining pressure (σ_3) (Fig. 1d). During earthquakes, the subgrade soil is subjected to a series of vibrating stress applications. These vibratory stresses may cause large deformation in soil structure and also lead to destructions on earthwork application with freeze-thaw cycles. To prevent this, influences of fibers and freeze-thaw cycles were determined for clay soil under earthquake loads in this study. Determination of dynamic soil properties is essential to analyze earthquake problems and their effects. Therefore, applying dynamic triaxial test is more suitable for performance of thawing soil subjected to dynamic load.

The summary of dynamic stress amplitudes and the general testing schema are presented in Tables 3 and 4, respectively. Dynamic triaxial tests were implemented on prepared specimens with multi-stage dynamic loading process under confining pressure 0.3 MPa, 0.4 MPa and 0.5 MPa. Dynamic loading was arranged to 40 levels varied from small to large and each level involved 30 loading cycles at a constant frequency of 1 Hz. Failure criteria of both unreinforced and fiber-reinforced specimens under dynamic loading were defined at shear strain of 20%.

3. Determination of dynamic parameters

The dynamic shear stress, τ_d and dynamic shear strain, γ_d of fiber-reinforced soil can be deduced from the following equations:

$$\tau_d = \sigma_d/2 \tag{2}$$

$$\gamma_d = \varepsilon_d(1 + \mu) \tag{3}$$

where σ_d is the axial dynamic shear stress obtained from experimental results, ε_d is the axial cyclic strain obtained from experimental results, and μ is the dynamic Poisson' ratio. Further, the repeated dynamic loading with the sine wave form was imposed on the specimen under different confining pressures in the axial direction. The axial force (σ_d) and the axial strain (ε_d) were measured by a data acquisition system during the dynamic triaxial test. The failure was called as the sum of the elastic strain and plastic strain equals to 20%.

Hardin-Drnevich used a hyperbolic model to describe the relationship between the dynamic shear stress and dynamic shear strain [32]. The Hardin model is expressed as follows:

$$\tau_i = \frac{\gamma_i}{a + b\gamma_i} \tag{4}$$

where a and b are described as the fitting parameters and $a > 0$ and $b > 0$.

Kondner-Zelasko studied the stress–strain curves of many soils, both

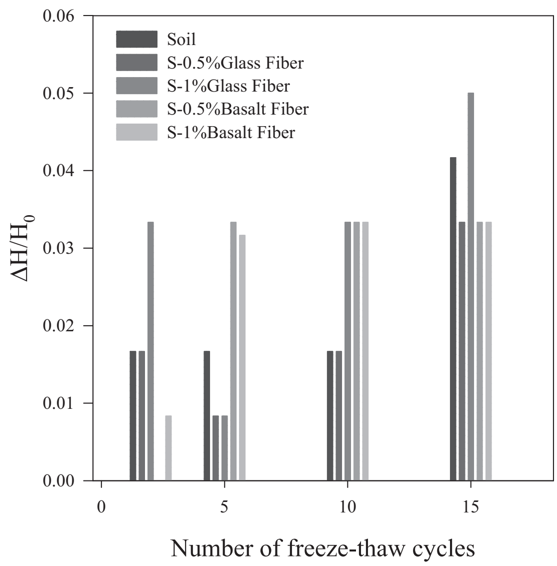

a. The *H* versus the number of freeze- thaw cycles

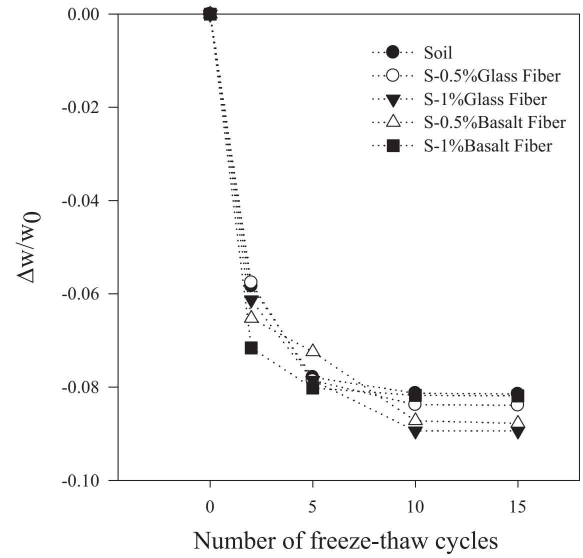

b. The *D* versus the number of freeze- thaw cycles

Fig. 3. Effects of freeze-thaw cycles on physical parameters of fiber-reinforced soil. a. The *H* versus the number of freeze- thaw cycles. b. The *D* versus the number of freeze- thaw cycles.

clay and sand can be expressed by hyperbolas as follows [33]:

$$\tau_i = f(\gamma) = \frac{G_i \gamma}{1 + (G_i/\tau_{ult})\gamma} \tag{5}$$

where G_i is initial tangent modulus at $\gamma \to 0$ and τ_{ult} is dynamic ultimate stress under dynamic loading.

Matasović and Vucetic (1993) noted that the Kondner-Zelasko model was not appropriate to describe the soil stress-strain behavior [34]. It is necessary to add some descriptive parameters to be more accurate. Therefore, two curve-fitting parameters were defined to obtain the best fitting curve for soil specimens in this research. With the addition of these two parameters, denoted β and n, the improved model assumes the following form:

$$\tau = f(\gamma) = \frac{G_i \gamma}{1 + \beta\left(\frac{\gamma}{\gamma_f}\right)^n} \tag{6}$$

where γ_f is the reference strain defined by Hardin-Drnevich (1972) [32].

The modified Kondner-Zelasko model (hereafter MKZ) was introduced to describe both unreinforced and fiber-reinforced soil specimens subjected to freeze-thaw cycles. These curve-fitting parameters operated form of initial loading curve in the range of shear strain between small values near failure [35].

Fig. 2 depicts the general hysteresis loop of the dynamic shear stress and dynamic shear strain of fiber-reinforced soil. The mean slope of loop was named as the dynamic shear modulus which can be expressed as the following form:

$$G_d = \frac{\overline{\tau}_d}{\overline{\gamma}_d} \tag{7}$$

where $\overline{\tau}_d$ is the amplitude of dynamic shear stress and $\overline{\gamma}_d$ is the amplitude of dynamic shear strain.

Considering both of the dynamic triaxial test results and curve-fitting constants, the relationships between dynamic shear modulus and shear strain were described by Hardin-Drnevich model in Eq. (8) and in Eq. (9) by MKZ model.

$$G_d = \frac{1}{a + b\gamma} \tag{8}$$

$$G_d = \frac{G_0}{1 + \beta\left(\frac{\gamma}{\gamma_f}\right)^n} \tag{9}$$

where G_d is dynamic shear modulus at $\gamma \to a$, G_o is the initial shear modulus.

The damping ratio (D_i) of unreinforced and fiber-reinforced specimens exposed freeze-thaw cycles can be computed from the following equation:

$$D_i = \frac{W_D}{4\pi W_S} \tag{10}$$

W_D is energy dissipated in one loading cycle and W_S is the maximum strain energy stored during the cycle. As illustrated in Fig. 2, the area inside the hysteresis loop is W_D, and the area of the triangle is W_S. Theoretically, at high strain ratio, nonlinearity between stress and strain causes an increment in damping ratio by increasing the strain amplitude.

4. Results and discussion

4.1. Effects of freeze-thaw cycles on the physical parameters of fiber-reinforced soil

In order to show effects of fibers on water content and height changes during freeze-thaw cycles, a number of freeze-thaw tests were carried out. Fig. 3a demonstrates the height changes of fibers versus the number of freeze-thaw cycles.

The reinforced soils with basalt and glass fibers were exhibited the different height changes under different numbers of freeze-thaw cycles. The 1% basalt fiber-reinforced soil showed about 50% mitigation on frost heave after two freeze-thaw cycles. The most remarkable effects of mitigation on the frost heave were observed on the specimens reinforced with 0.5% and 1% glass fibers after five freeze-thaw cycles. Besides, 0.5% glass fiber-reinforced soil exhibited better mitigation on the frost heave than 1% glass fiber-reinforced soil for all freeze-thaw cycles. Moreover, after the maximum freeze-thaw cycle, the mitigation

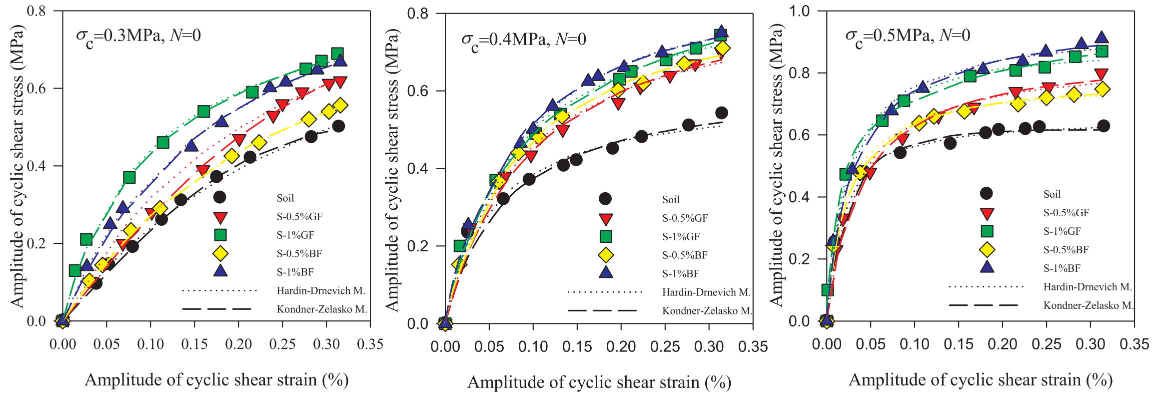

a. N=0, χ=0, 0.5 and 1%, σ_c=0.3, 0.4 and 0.5 MPa

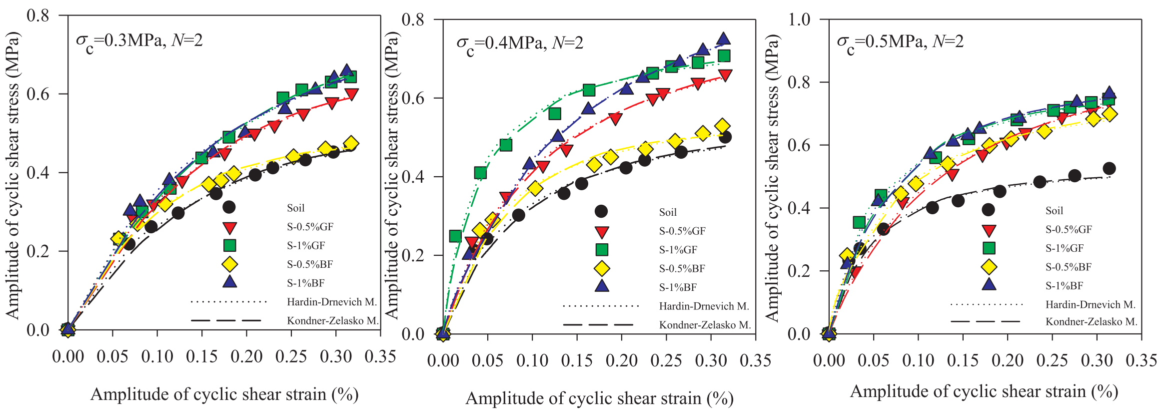

b. N=2, χ=0, 0.5 and 1%, σ_c=0.3, 0.4 and 0.5 MPa

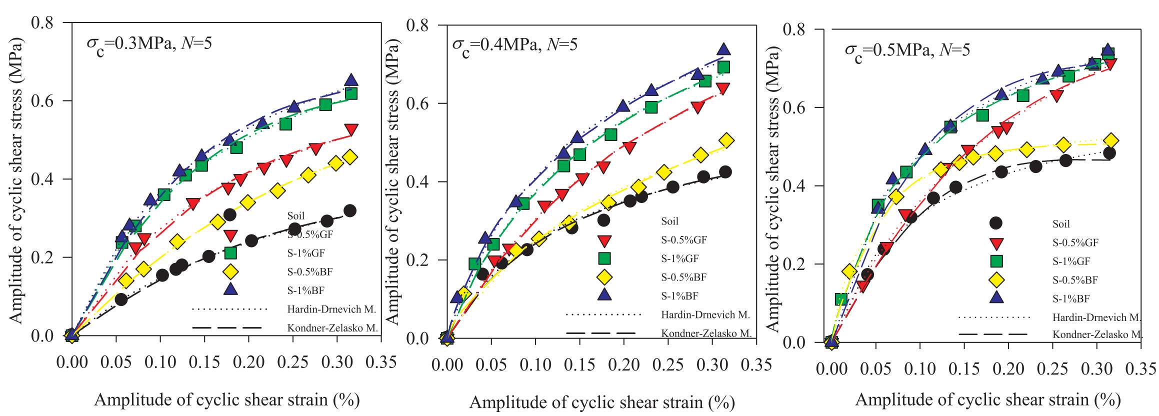

c. N=5, χ=0, 0.5 and 1%, σ_c=0.3, 0.4 and 0.5 MPa

Fig. 4. Relationships between τ_d and γ_d obtained from experimental results, the Hardin-Drnevich model and the MKZ model for different N, σ_c and χ. a. $N = 0$, $\chi = 0\%$, 0.5% and 1%, $\sigma_c = 0.3$, 0.4 and 0.5 MPa. b. $N = 2$, $\chi = 0\%$, 0.5% and 1%, $\sigma_c = 0.3$, 0.4 and 0.5 MPa. c. $N = 5$, $\chi = 0\%$, 0.5% and 1%, $\sigma_c = 0.3$, 0.4 and 0.5 MPa. d. $N = 10$, $\chi = 0\%$, 0.5% and 1%, $\sigma_c = 0.3$, 0.4 and 0.5 MPa. e. $N = 15$, $\chi = 0\%$, 0.5% and 1%, $\sigma_c = 0.3$, 0.4 and 0.5 MPa.

of frost heave was observed about 19% on both the 0.5% glass fiber-reinforced soil and the 0.5% basalt fiber reinforced soil. Furthermore, the frost heave was mitigated by about 20% with the addition of 1% basalt fiber in soil.

Moreover, Fig. 3b shows the D versus number of freeze-thaw cycles for both unreinforced and fiber-reinforced specimens. At the beginning, the water content of all soil specimens reduced with increasing number of freeze-thaw cycles, and then slowly steadied after tenth freezing-thawing cycles. Compared with unreinforced soil, it is observed that the water content decreased with the inclusion of fiber content. It is mainly because woven fibers like basalt and glass fibers can drain water in the soil volume. However, this reduction is negligible.

According to Fig. 3, the tenth freeze-thaw cycle can be taken as a critical cycle in present study, after which the height of all soil specimens reached a constant, and the soil specimens reached a new dynamic stability in their textures.

4.2. Effects of freeze-thaw cycles and confining pressure on dynamic shear stress of unreinforced and fiber-reinforced soil

The relationships between τ_d -γ_d obtained from experimental results, the Hardin-Drnevich model and the MKZ hyperbolic model were

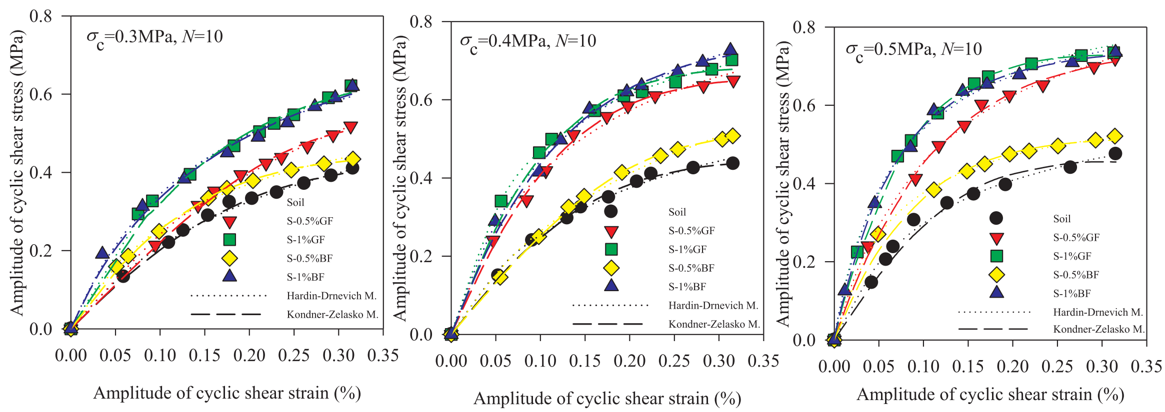

d. N=10, χ=0, 0.5 and 1%, σ_c=0.3, 0.4 and 0.5 MPa

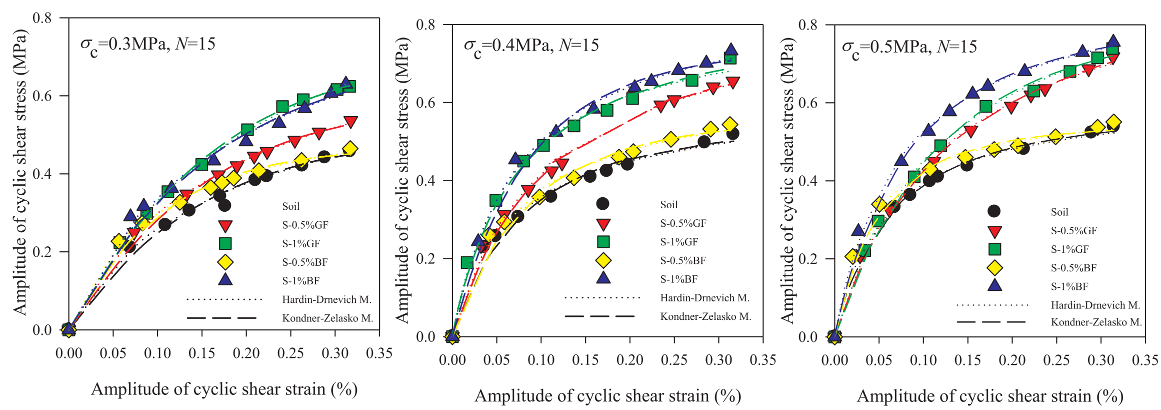

e. N=15, χ=0, 0.5 and 1%, σ_c=0.3, 0.4 and 0.5 MPa

Fig. 4. (*continued*)

Table 5
Regression analysis constants *a* and *b* for Eq. (4).

Test No	**0 F-T cycle**		**2 F-T cycles**		**5 F-T cycle**		**10 F-T cycle**		**15 F-T cycle**	
σ_c = 0.3 MPa	*a*	*b*	*a*	*b*	*a*	*b*	*a*	*b*	*a*	*b*
Soil	0.3293	0.9201	0.2329	1.4383	0.5255	1.5712	0.3380	1.3811	0.2467	1.4306
Soil-0.5%Glass F.	0.2979	0.6387	0.1963	1.0624	0.2421	1.1902	0.3269	0.8867	0.2184	1.1991
Soil-1%Glass F.	0.1138	1.1239	0.2075	0.8749	0.1797	1.0742	0.1916	1.0422	0.2100	0.9170
Soil-0.5%Basalt F.	0.2687	0.9600	0.1623	1.6281	0.3970	0.9518	0.2375	1.5108	0.1657	1.6701
Soil-1%Basalt F.	0.1766	0.9395	0.1822	0.9876	0.1684	1.0393	0.1785	1.1158	0.1920	1.0315
Test No	0 F-T cycle		2 F-T cycles		5 F-T cycle		10 F-T cycle		15 F-T cycle	
σ_c = 0.4 MPa	*a*	*b*	*a*	*b*	*a*	*b*	*a*	*b*	*a*	*b*
Soil	0.0918	1.6724	0.1313	1.6958	0.2358	1.6797	0.2487	1.4283	0.1156	1.6414
Soil-0.5%Glass F.	0.1027	1.1587	0.1229	1.1473	0.2460	0.8082	0.1382	1.0566	0.1237	1.1561
Soil-1%Glass F.	0.0907	1.1021	0.0480	1.3029	0.1713	0.9385	0.1008	1.1263	0.0822	1.2079
Soil-0.5%Basalt F.	0.0969	1.1414	0.1008	1.6468	0.2847	1.1734	0.2725	1.0675	0.1126	1.5292
Soil-1%Basalt F.	0.0868	1.0765	0.1333	0.9370	0.1464	0.9463	0.1282	0.9719	0.0857	1.1307
Test No	0 F-T cycle		2 F-T cycles		5 F-T cycle		10 F-T cycle		15 F-T cycle	
σ_c = 0.5 MPa	*a*	*b*	*a*	*b*	*a*	*b*	*a*	*b*	*a*	*b*
Soil	0.0243	1.5244	0.0713	1.7881	0.1500	1.5666	0.1810	1.5418	0.0914	1.6233
Soil-0.5%Glass F.	0.0393	1.1783	0.1241	0.9883	0.1958	0.7915	0.1191	1.0067	0.1288	1.0171
Soil-1%Glass F.	0.0232	1.1158	0.0644	1.1585	0.0995	1.0865	0.0754	1.0852	0.1240	0.9876
Soil-0.5%Basalt F.	0.0266	1.2912	0.0761	1.2319	0.0737	1.6867	0.1077	1.5825	0.0678	1.6660
Soil-1%Basalt F.	0.0277	1.0506	0.0729	1.1011	0.0995	1.0598	0.0750	1.1050	0.0816	1.0838

F-T: Freeze-thaw cycles.

presented in Fig. 4a–e. Each series of the curves depicts the results of different confining pressure and fiber content.

As shown in Fig. 4a–e, when the dynamic shear strain is smaller than about 0.02%, the τ_d -γ_d curves exhibit linear behavior. However, when the dynamic shear strain is higher than 0.02%, the τ_d -γ_d curves show nonlinear behavior. Moreover, the volume fractions of fibers and the freeze-thaw cycles obviously influenced the strain levels and the maximum amplitude values. The dynamic axial stress increased with both the fiber content and dynamic shear strain. The dynamic axial stresses of all soil specimens decreased after freeze-thaw cycles, and less

Table 6
Regression analysis constants β and n for Eq. (6).

Test No	0 F-T cycle		2 F-T cycles		5 F-T cycle		10 F-T cycle		15 F-T cycle	
σ_c = 0.3 MPa	β	n	β	n	β	n	β	n	β	n
Soil	0.5546	2.1617	1.1735	1.4251	0.6324	1.4818	0.7647	1.7084	1.1568	1.3640
Soil + 0.5%Glass F.	0.4711	1.5562	1.0559	1.4275	0.9519	1.3770	0.3931	2.5508	1.0493	1.3947
Soil + 1%Glass F.	3.2176	0.9332	0.9561	1.3553	1.1973	1.4102	1.0271	1.3880	0.9635	1.4047
Soil + 0.5%Basalt F.	0.9429	1.1686	1.8094	1.3616	0.5913	1.2288	1.2965	1.5025	1.8234	1.3452
Soil + 1%Basalt F.	1.3929	1.1138	1.1222	1.2414	1.2122	1.4244	1.8398	0.9567	1.1341	1.2248
Test No	0 F-T cycle		2 F-T cycles		5 F-T cycle		10 F-T cycle		15 F-T cycle	
σ_c = 0.4 MPa	β	n	β	n	β	n	β	n	β	n
Soil	4.4208	1.0134	2.9108	1.0949	2.0009	0.9962	1.0533	1.7273	3.0778	1.1280
Soil + 0.5%Glass F.	3.0621	1.0031	2.5225	1.0303	0.8636	1.1062	1.5093	1.5281	2.5233	1.0498
Soil + 1%Glass F.	4.1733	0.9127	7.1716	1.0038	1.7961	0.9162	1.8311	1.4585	4.2119	0.9922
Soil + 0.5%Basalt F.	3.3661	1.0231	2.9534	1.2247	2.8606	0.6166	0.6681	2.1659	2.7243	1.1764
Soil + 1%Basalt F.	3.1301	1.0740	1.9299	1.0464	2.8992	0.7874	1.5686	1.3266	2.7095	1.1929
Test No	0 F-T cycle		2 F-T cycles		5 F-T cycle		10 F-T cycle		15 F-T cycle	
σ_c = 0.5 MPa	β	n	β	n	β	n	β	n	β	n
Soil	12.4337	1.0824	5.2797	1.0879	1.7985	1.6616	1.3984	1.7588	4.3481	1.0546
Soil + 0.5%Glass F.	7.6451	1.0099	2.0324	1.0665	0.8523	1.4583	1.8073	1.2918	2.2404	1.0055
Soil + 1%Glass F.	30.1226	0.8825	3.4890	1.1706	3.4477	0.9643	2.7332	1.3590	1.8476	1.1856
Soil + 0.5%Basalt F.	12.5320	1.0053	4.5701	0.9827	4.5590	1.2010	2.3855	1.3452	4.9970	1.1200
Soil + 1%Basalt F.	11.2657	0.9712	3.4694	1.1189	1.8331	1.4230	3.5665	1.1677	3.2573	1.0817

F-T: Freeze-thaw cycles.

reduction was observed in the fiber-reinforced soil.

The maximum amplitude increased with strain level for unreinforced and fiber-reinforced specimens because soil tended to be strain softening with the increase of strain level. As presented in Table 2, the breaking strength and modulus of elasticity of basalt fiber were higher than the glass fiber, which can improve the resistance more efficiently. However, the breaking extension of basalt fiber was less than glass fiber and this can be stated as the transition from their strain-softening to strain-hardening is smaller than glass fiber reinforced specimens. Besides, the τ_d -γ_d relation in each figure increased with confining pressure (σ_c = 0.3 MPa, 0.4 MPa and 0.5 MPa).

The relationship between dynamic shear stress and strain predicted by the Hardin-Drnevich model and the MKZ model fitted well with experimental results. The curve-fitting constants *a*, *b* and β, *n* are shown in Table 5 for the Hardin-Drnevich model and in Table 6 for MKZ model.

4.3. Effects of freeze-thaw cycles on dynamic shear modulus of unreinforced and fiber-reinforced soil

The relationships between normalized dynamic shear modulus, G_d/G_0 and shear strain amplitude, γ of unreinforced and fiber-reinforced soil subjected to different freeze-thaw cycles were presented in Fig. 5a–e. The results showed that the G_d increased with fiber volume fraction at a constant confining pressure and decreased with increasing shear strain. 1% glass fiber-reinforced soil and 1% basalt fiber-reinforced soil exhibited the most significant impacts on the G_d. Also, the increase in the confining pressure causes to increase the friction between soil particles. Thus, the maximum dynamic elastic modulus of soil are raised. Moreover, the cohesion reduction, melting, the migration and increase of water in mixture, plastic flow can be seen on the soil specimen with the increasing of the confining pressure [19]. These results are in good agreement with the findings of Maher and Woods (1990), which suggested that for dynamic loads as fiber content increased, the rigidity of the composite material increased [36]. The shear modulus increases with the addition of the fiber; however, the G_d/G_0 plots of both fibers and their ratios showed a reduction in stiffness at small confining pressure. On the other hand, the values of the G_d/G_0 increased with increasing of the confining pressures for a given percentage of fiber. This results from an increase in material stiffness due to an increase in confining pressure.

After freeze-thaw cycles, reduction trend on dynamic shear modulus increased with the addition of the basalt and glass fibers. However, the increment is relatively small after tenth freeze-thaw cycles which indicates that, soil texture has obtained a new dynamic equilibrium. Onward moving was used to describe supplied pore water moving from middle to the top of soil cell during freezing period. Similarly, if the water is migrating from the top to the middle side during thawing period, this is called reversed moving. In soil textures, more onward moving can be observed. After a number of freeze-thaw cycles, the quantity of water moving between onward and reversed moving will reach a dynamic state.

The G_d of unreinforced soil decreased about 6.4% at shear strain of γ = 0.05% after tenth freeze-thaw cycle. At this strain level and the freeze-thaw cycle, the G_d of 0.5% glass fiber-reinforced soil decreased by 21.2%, for 1% glass fiber-reinforced soil decreased by 30.3%, for 0.5% basalt fiber-reinforced soil decreased by 1.3%, and for 1% basalt fiber-reinforced soil decreased by 3.7%.

Moreover, the Hardin-Drnevich (HD) and MKZ hyperbolic models reflect well relations between the G_d and γ by comparing with the experimental data. Table 7 shows the comparison of the Hardin-Drnevich model and the MKZ hyperbolic model after experienced zeroth and tenth freeze-thaw cycles for shear strain level of γ = 0.05% and σ_c = 0.3 MPa.

The G_d of unreinforced soil at the dynamic shear strain of γ = 0.05%, σ_c = 0.3 MPa and N = 0 was experimentally determined 239.17 MPa, and the τ_d was observed 0.145 MPa. The G_d of the unreinforced soil is 264.46 MPa based on the Hardin-Drnevich model and is 241.36 MPa based on the MKZ hyperbolic model. The predicted results were greater than the experimental results. The Hardin-Drnevich model has a significant effect on the G_d than the MKZ hyperbolic model. The τ_d of the unreinforced soil is 0.143 MPa based on the Hardin-Drnevich model and is 0.128 MPa based on the MKZ hyperbolic model. Based on this result of the τ_d, the MKZ hyperbolic model shows more reduction effect on the G_d than the Hardin-Drnevich model. This indicates that the coefficients of τ_d may be overestimated for both models.

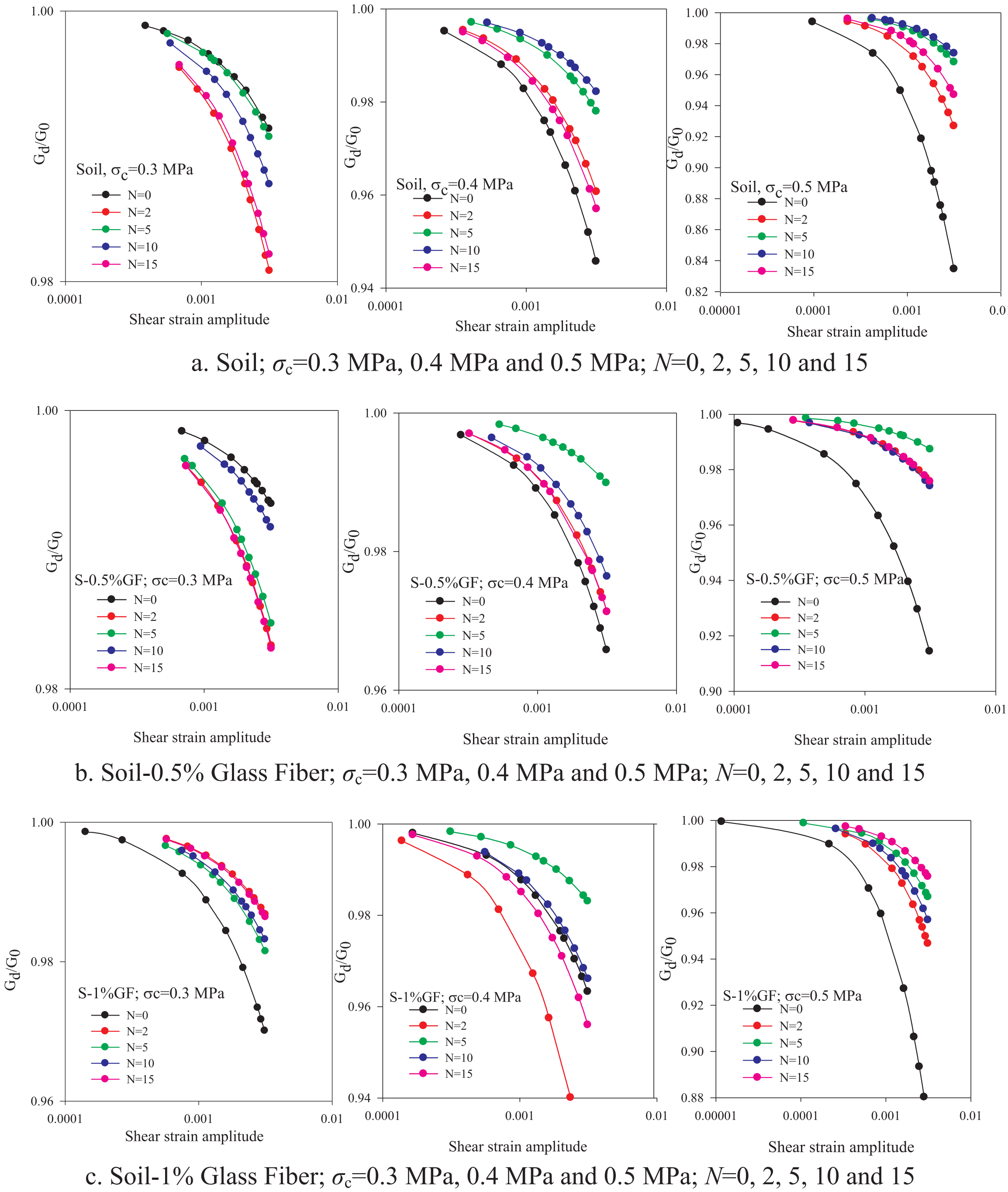

Fig. 5. Relationships between G_d/G_0 and γ for different σ_c, N and χ. a. $N = 0$, χ = 0%, 0.5% and 1%, σ_c = 0.3, 0.4 and 0.5 MPa. b. $N = 2$, χ = 0%, 0.5% and 1%, σ_c = 0.3, 0.4 and 0.5 MPa. c. $N = 5$, χ = 0%, 0.5% and 1%, σ_c = 0.3, 0.4 and 0.5 MPa. d. $N = 10$, χ = 0%, 0.5% and 1%, σ_c = 0.3, 0.4 and 0.5 MPa. e. $N = 15$, χ = 0%, 0.5% and 1%, σ_c = 0.3, 0.4 and 0.5 MPa.

4.4. *Effects of freeze-thaw cycles on damping ratios of unreinforced and fiber-reinforced soil*

The relationships between damping ratio (D_i) and shear strain amplitude of unreinforced and fiber-reinforced soil for different numbers of freeze-thaw cycles were presented in Fig. 6a–e. The damping ratio increased with increasing of fiber content under all confining pressures. This state is related to an increment of displacement and plastic strain under the dynamic shear stress. Further, damping ratios after freeze-thaw cycles increased with fiber contents. Also, variation of confining pressure has little effect on the damping ratio of unreinforced and reinforced soil with various amounts of fiber. This result is in good agreement with the previous studied results by Naeini and Gholampoor (2014) [16].

5. The theoretical analytical formulations of nonlinear elasticity

5.1. *Identification of parameters*

When the soil subjects to severe ground action, it exhibits anisotropic, nonlinear and time-dependent behavior. Under natural condition, soil is subjected to loading, unloading and reloading processes. It shows a non-linear behavior before failure with stress related to stiffness [22].

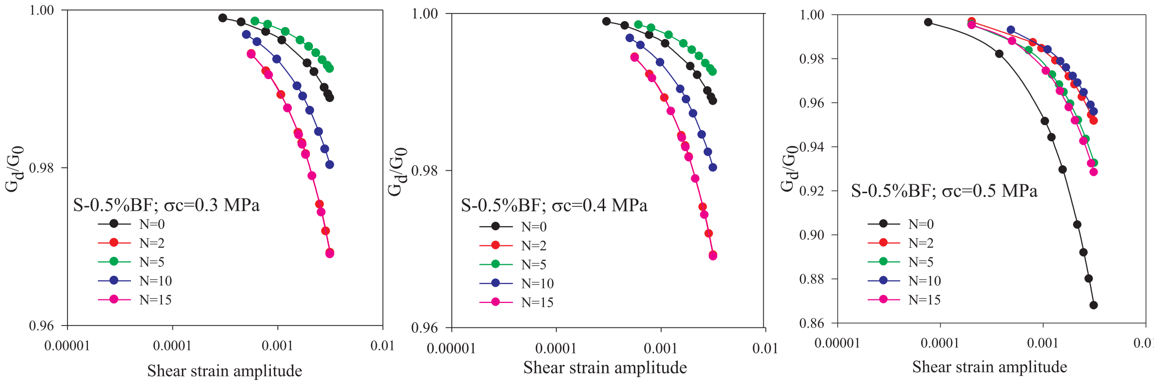

d. Soil-0.5% Basalt Fiber; σ_c=0.3 MPa, 0.4 MPa and 0.5 MPa; N=0, 2, 5, 10 and 15

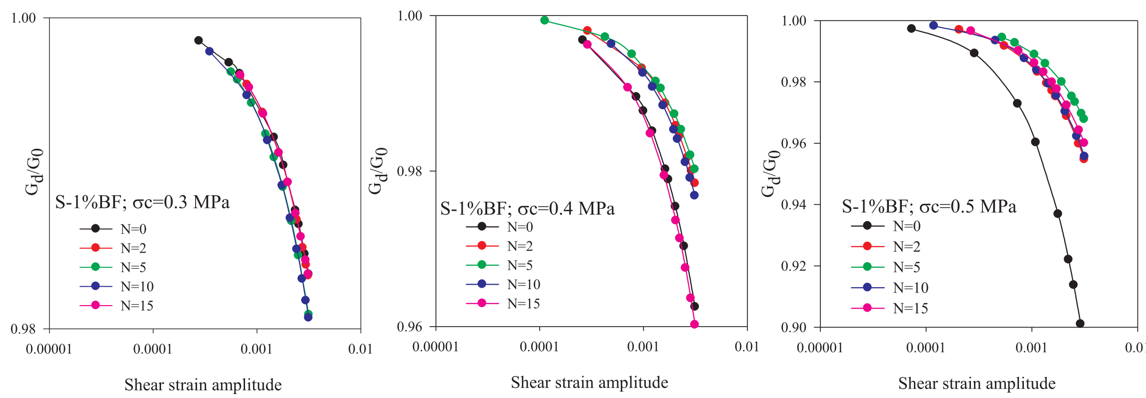

e. Soil-1% Basalt Fiber; σ_c=0.3 MPa, 0.4 MPa and 0.5 MPa; N=0, 2, 5, 10 and 15

Fig. 5. (*continued*)

Table 7
Comparison of the Hardin-Drnevich model and the MKZ hyperbolic model.

N = 0, γ = 0.0005, σ_c = 0.3 MPa		Tested materials				
Values	Model	S	S-0.5G	S-1G	S-0.5B	S-1B
τ_d **(MPa)**	HD	0.143	0.238	0.361	0.156	0.238
	MKZ	0.128	0.191	0.344	0.15	0.228
G_d **(MPa)**	HD	264.46	293.71	474.36	320.24	415.08
	MKZ	241.36	280.76	470.34	308.65	403.04
N = 10, γ = 0.0005, σ_c = 0.3 MPa		Tested materials				
Values	Model	S	S-0.5G	S-1G	S-0.5B	S-1B
τ_d **(MPa)**	HD	0.141	0.18	0.229	0.162	0.172
	MKZ	0.127	0.17	0.207	0.147	0.166
G_d **(MPa)**	HD	238.09	247.41	371.13	318.03	390.94
	MKZ	214.47	225.86	342.32	289.04	389.32

The fiber-reinforced soil exposed to dynamic axial stress exhibits nonlinear elastic behavior. The relationship between shear stress and shear strain can be defined with regard to the second invariants of deviatoric tensors [23];

$$\sigma^s = G\varepsilon^s \tag{11}$$

σ^s ($\equiv \sqrt{3I_D^2}$) is a shear stress constant related the second invariant of deviatoric stress tensor I_D^2($\equiv \sigma_{ij}^D\sigma_{ij}^D/2$, σ_{ij}^D is deviatoric stress tensor); the G is the second order tensor of elasticity, ε^s ($\equiv \sqrt{3J_D^2}$) is a shear strain invariant associated with the second invariant of strain deviatoric tensor J_D^2($\equiv \varepsilon_{ij}^D\varepsilon_{ij}^D/2$, ε_{ij}^D is deviatoric strain tensor).

The deviatoric stress strain relations $\sigma^{Ds} = G\varepsilon^{Ds}$ can be stated in terms of stress and stress invariants:

$$\sqrt{I_2^D} \equiv G\sqrt{J_2^D} \tag{12}$$

In principal quasi-triaxial stress space, $\sigma_1 \ddagger \sigma_2 = \sigma_3$, $\varepsilon_1 \ddagger \varepsilon_2 = \varepsilon_3$ and the stress-strain relations in Eq. (12) reduce to:

$$\sigma_1 - \sigma_3 = G(\varepsilon_1 - \varepsilon_3) \tag{13}$$

σ_1- σ_3 is difference between the maximum and the minimum principal stresses, ε_1- ε_3 is difference of the maximum and the minimum principal strains. For conventional dynamic triaxial test, Eq. (13) can be clarified to:

$$\sigma_1 - \sigma_3 = G\varepsilon_1 \tag{14}$$

In this research, theoretical analytical formulations were used to calculate dynamic shear modulus (G_d) considering dynamic triaxial test results of unreinforced and fiber-reinforced soil specimens subjected freeze-thaw cycles. It can be stated as a function of variation of fiber fraction, number of freeze-thaw cycles, initial water content, and confining pressure shown as follows:

$$G_d = F_o \times f(e^N + e) \times f(1 + \chi) \times f(w) \times f(\sigma_c/P_a) \times P_a \tag{15}$$

F_o is the model parameter, $f(e^N + e)$, $f(1 + \chi)$, $f(w)$, and $f(\sigma_c/P_a)$ are the functions of number of freeze-thaw cycles N, variation of fiber fraction χ, initial water content w, and confining pressure σ_c, respectively, where P_a is the atmospheric pressure (taken equal to 0.101 MPa), e is the mathematical constant (taken equal to 2.72), w and χ are expressed as percentages (%), and σ_c and G_d are expressed in MPa.

The coefficients of the best-fit hyperbola for dynamic shear stress-strain curve are calculated from the plot of the $1/G_d - \gamma_d$. The best fit straight line on this transformed plot corresponds to the best-fit hyperbola on the dynamic stress-strain plots (Fig. 7a–e).

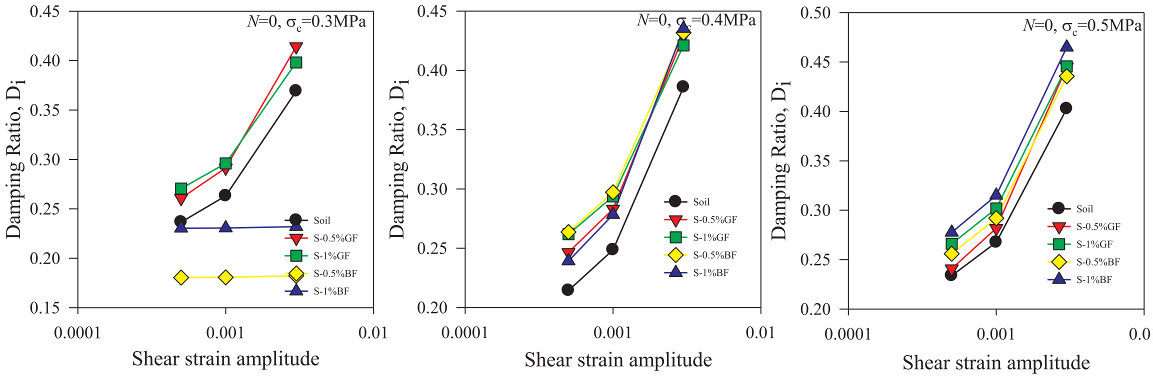

a. N=0, χ=0, 0.5 and 1%, σ_c=0.3, 0.4 and 0.5 MPa

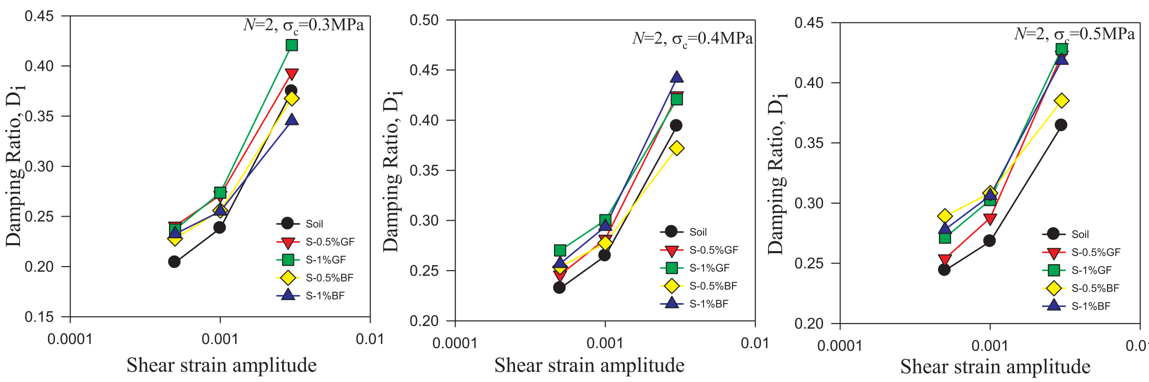

b. N=2, χ=0, 0.5 and 1%, σ_c=0.3, 0.4 and 0.5 MPa

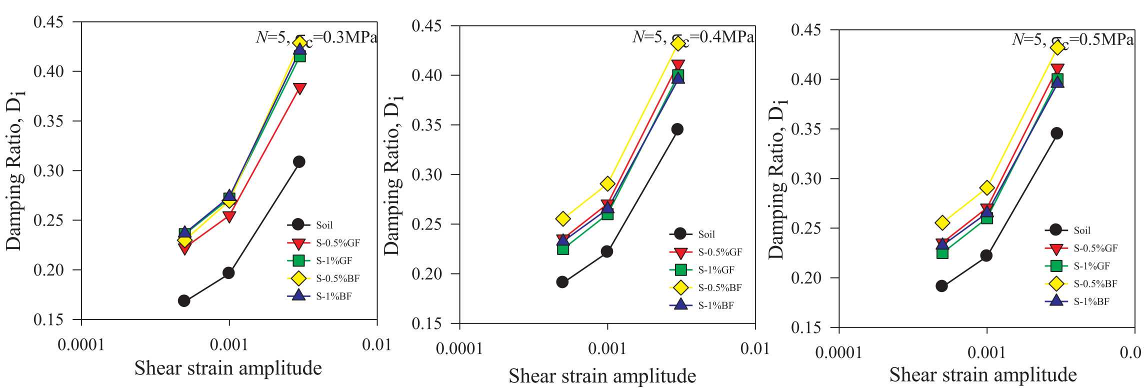

c. N=5, χ=0, 0.5 and 1%, σ_c=0.3, 0.4 and 0.5 MPa

Fig. 6. Effects of number of freeze-thaw cycles, confining pressure and fiber content on damping ratio.

To describe the dynamic shear stress-strain relationship, the function of G_d *is* explained by using the following equation:

$$G_d = 1/[A(F_o \times f(e^N + e) \times f(1+\chi) \times f(w) \times f(\sigma_c/P_a) \times P_a) + B((F_o \times f(1+N) \times f(e^N + e) \times f(w) \times f(\sigma_c/P_a) \times P_a)\,\varepsilon^s] \quad (16)$$

A and B are both a function of N, χ, w and σ_c. The functions of $1/A$ and $1/B$ present the secant tangential shear modulus and the dynamic ultimate stress, respectively.

The term G_d in Eq. (15) can be clarified to:

$$G_d = \sigma_d/\varepsilon_d = 1/[A(N, \chi, w, \sigma_c) + B(N, \chi, w, \sigma_c)\,\varepsilon^s] \quad (17)$$

or $1/G_d$ can be stated by

$$1/G_d = \varepsilon_d/\sigma_d = A(N, \chi, w, \sigma_c) + B(N, \chi, w, \sigma_c)\,\varepsilon^s \quad (18)$$

The linear relation (Eq. (17)) allows one to calibrate constitutive parameters simply from experimental curves. In this study, the functions of A and B in Eq. (17) or Eq. (18) are assumed to be expressed as follows:

$$A(N, \chi, w, \sigma_c) = (c_0/P_a)(e^N + e)^{c1}(1+\chi)^{c2}(w)^{c3}(\sigma_c/P)^{c4} \quad (19)$$

$$B(N, \chi, w, \sigma_c) = (d_0/P_a)(e^N + e)^{d1}(1+\chi)^{d2}(w)^{d3}(\sigma_c/P_a)^{d4} \quad (20)$$

c_i (i = 0,…,4) and d_i (i = 0,…,4) are constants and are to be obtained from dynamic triaxial tests. P_a is atmospheric pressure (MPa) for dimensional coefficients (c_0/P_a and d_0/P_a) and dimensionless terms (σ_c/P_a) in Eqs. (19) and (20).

The hyperbolic curve for dynamic shear stress-strain is employed to determine constitutive parameters A and B linearly.

A linear regression for multi parameters is assumed to determine the constitutive parameters: c_i (i = 0….4) and d_i (i = 0….4). Thus, each function was determined by Eqs. (21) and (22):

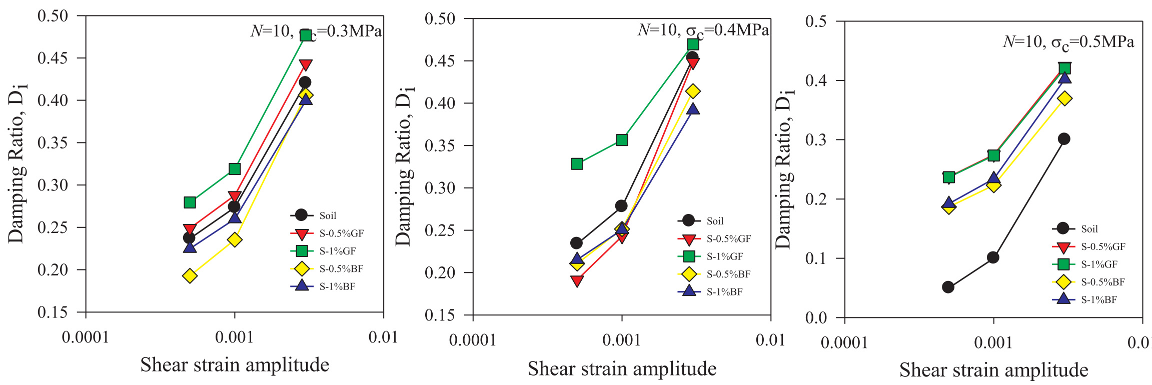

d. N=10, χ=0, 0.5 and 1%, σ_c=0.3, 0.4 and 0.5 MPa

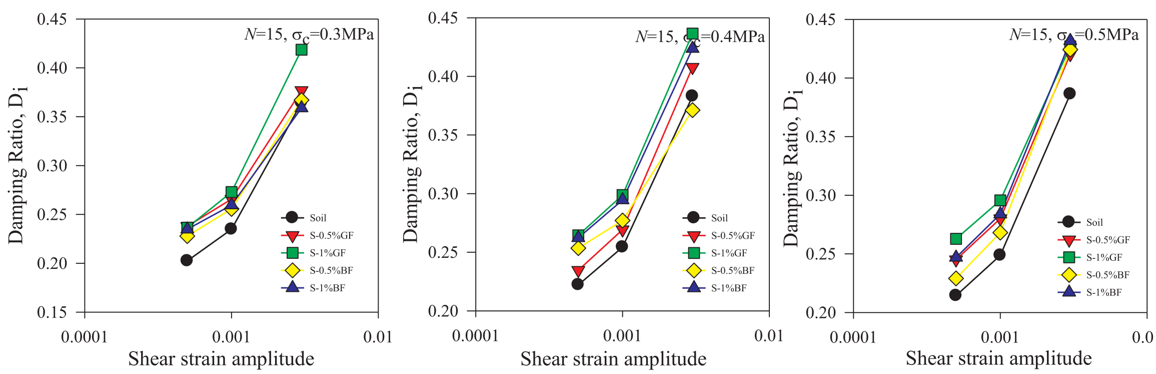

e. N=15, χ=0, 0.5 and 1%, σ_c=0.3, 0.4 and 0.5 MPa

Fig. 6. (*continued*)

$$\log A = \log(c_0/P_a) + c_1\log(e^N + e) + c_2\log(1+\chi) + c_3\log(w) + c_4\log(\sigma_c/P_a) \tag{21}$$

$$\log B = \log(d_0/P_a) + d_1\log(e^N + e) + d_2\log(1+\chi) + d_3\log(w) + d_4\log(\sigma_c/P_a) \tag{22}$$

The linear regression results of the coefficients (c_i and d_i) are presented in Table 8. Moreover, the functions of A and B were explained by Eqs. (23) and (24):

$$A = 1/G_d = 1.58\text{x}10^{-5}(e^{-0.054} + e)(1+\chi)^{-47.99}(w)^{-9.86}(\sigma_c/P_a)^{-2.07}P_a \tag{23}$$

$$B = 1/\sigma_{ult} = 4.04\text{x}10^{-1}(e^{-0.009} + e)(1+\chi)^{-41.19}(w)^{-2.37}(\sigma_c/P_a)^{-0.43}Pa \tag{24}$$

Eqs. (23) and (24) represent new expression of the dynamic shear modulus of unreinforced and fiber-reinforced specimens exposed to freeze-thaw cycles at strain levels studied. To investigate the effects of calibrated parameters on the function A and function B obtained from the formulations, function parameters, f, were introduced as f^A and f^B. From Eqs. (23) and (24), for fiber reinforcement, the functions of the f^A and the f^B can be written as $f_\chi^A = A(\sigma_c, N, w, \chi)/A(\sigma_c, N, w, 0)$ and the $f_\chi^B = B(\sigma_c, N, w, \chi)/B(\sigma_c, N, w, 0)$. Considering the outputs of these equations presented in Eqs. (23) and (24), the functions of the f_χ^A and the f_χ^B can be shown as individual functions: $f_\chi^A = (1+\chi)^{-47.99}$, $f_\chi^B = (1+\chi)^{-41.19}$. Similarly, to investigate the effects of the calibrated parameters, the functions of $f_{\sigma c}$, f_N and f_w are defined for the confining pressures, freeze-thaw cycles and water content, respectively. Table 9 shows that each impact function has independent influences on the fiber-reinforced soil.

According to Table 9, the impact functions of the fiber volume fraction, f_χ^A and f_χ^B, for both A ($1/G_d$) and B ($1/\sigma_{ult}$) have higher values than the others. Thus, the presence of fibers in clay soil shows a significant effect on the shear modulus and dynamic stress. Also, the similar influences on the A are seen on the impact functions of σ_c, N, w. Besides, when the confining pressure, freeze-thaw cycles and water content increase, the increase ratio of the A is faster than the increase ratio of the B. Namely, the $1/G_d$ is more sensitive against to changes of the confining pressure, the freeze-thaw cycles and the water content than $1/\sigma_{ult}$.

5.2. Statistical evaluation of nonlinear model performance

In this study, evaluation of the theoretical analytical formulations is based on three performance parameters: root mean square error (RMSE), maximum relative error (MRE) and determination coefficients (R^2).

The RMSE was calculated using the equation:

$$RMSE = \sqrt{\frac{\sum_{i=1}^{n}(f_{mi} - f_{ci})^2}{k}} \tag{25}$$

f_{mi} is the experimental dynamic parameter, f_{ci} is the predicted value k=n-1 if n < 30 and k=n if n > 30, n is the number of data. The MRE was calculated from the equation:

$$MRE = \max_{i=1,2..n}\left\{\left|\frac{(f_{mi} - f_{ci})}{f_{mi}}\right|100\%\right\} \tag{26}$$

Fig. 8a–b demonstrates the comparisons of parameters A ($1/G_d$) and B ($1/\sigma_{ult}$) with experimental results.

The results showed that the theoretical formulations could fit well the $1/G_D$ and $1/\sigma_{ult}$ of all soil specimens with R^2 = 0.756 and R^2 =

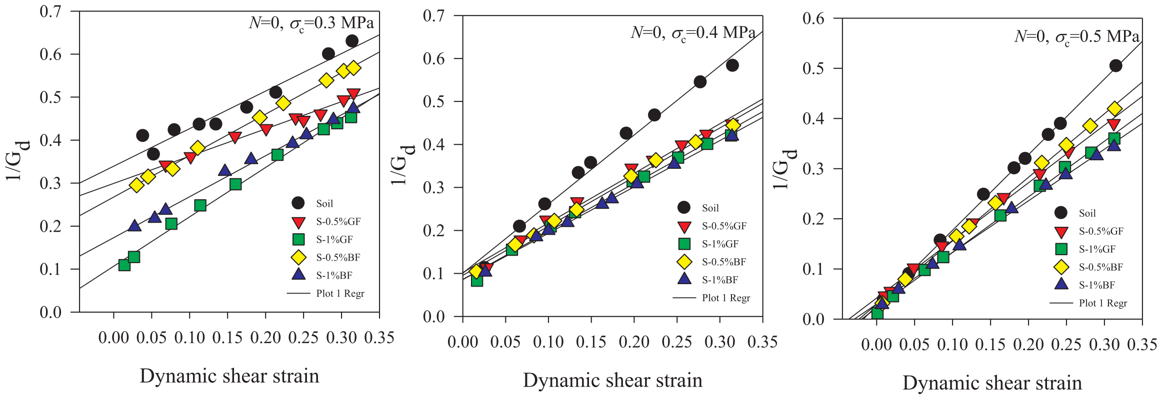

a. N=0, χ=0, 0.5 and 1%, σ_c=0.3, 0.4 and 0.5 MPa

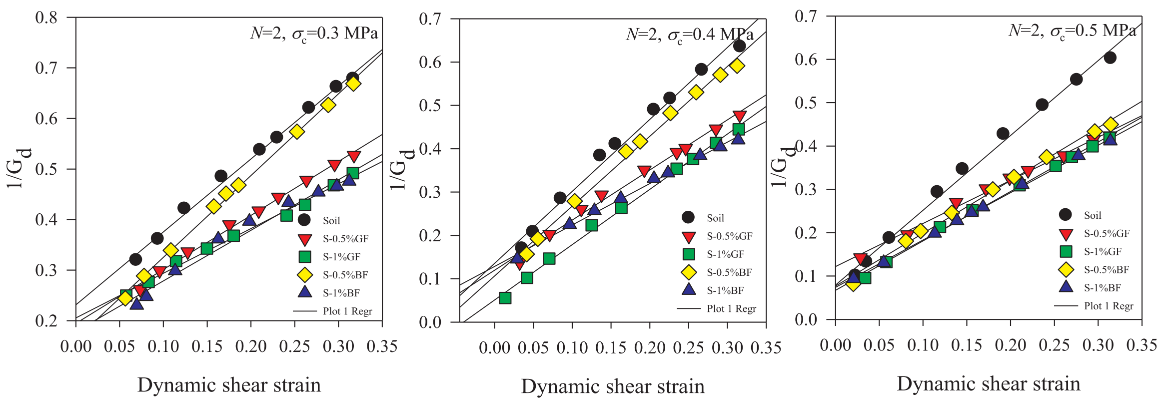

b. N=2, χ=0, 0.5 and 1%, σ_c=0.3, 0.4 and 0.5 MPa

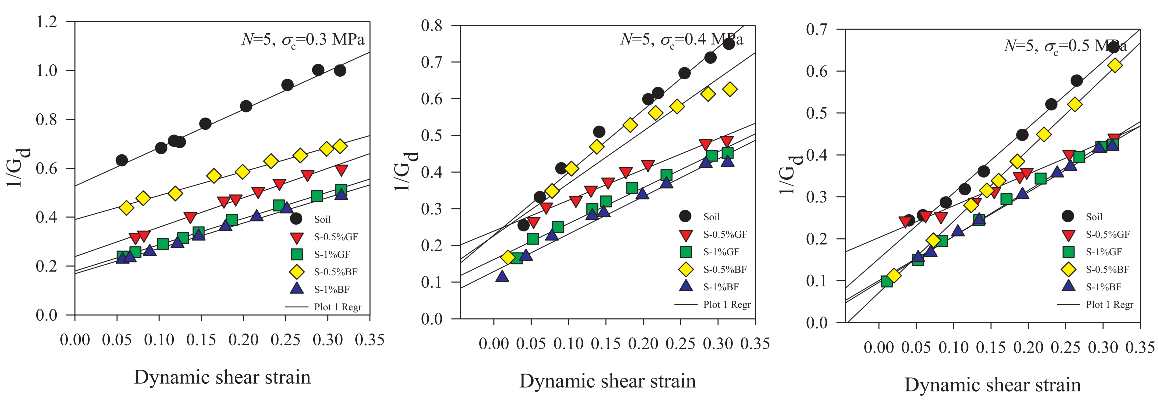

c. N=5, χ=0, 0.5 and 1%, σ_c=0.3, 0.4 and 0.5 MPa

Fig. 7. Relationships between $1/G_i$ and γ_d with different χ, σ_c and N. a. $N = 0$, $\chi =$ 0%, 0.5% and 1%, $\sigma_c = 0.3$, 0.4 and 0.5 MPa. b. $N = 2$, $\chi =$ 0%, 0.5% and 1%, $\sigma_c = 0.3$, 0.4 and 0.5 MPa. c. $N = 5$, $\chi =$ 0%, 0.5% and 1%, $\sigma_c = 0.3$, 0.4 and 0.5 MPa. d. $N = 10$, $\chi =$ 0%, 0.5% and 1%, $\sigma_c = 0.3$, 0.4 and 0.5 MPa. e. $N = 15$, $\chi =$ 0%, 0.5% and 1%, $\sigma_c = 0.3$, 0.4 and 0.5 MPa.

0.794, respectively (Fig. 8). The R^2 showed that predicted and experimental results are affined for both features.

Table 10 shows the values of the RSME and the MRE of predicted $1/G_D$ and $1/\sigma_{ult}$ obtained from formulations. The relatively meaningful determination coefficients showed that there was a remarkable relationship between the results of theoretical analytical formulations and experimental of the $1/G_D$ and the $1/\sigma_{ult}$. This is affirmed by the values of the RMSE (4.95×10^{-5}, 1.14×10^{-2} for $1/G_D$ and $1/\sigma_{ult}$, respectively) and the MRE (23.80%, 7.12% $1/G_D$ and $1/\sigma_{ult}$, respectively) using all 75 data.

The relationship between predicted and measured values of the RMSE and the MRE is good with minor deviations. It was observed that the lowest RMSE and MRE were with respect to basalt fiber-reinforced soil specimens after 15 freeze-thaw cycles. Furthermore, the trend lines of the RMSE and the MRE showed decreasing trend when the soil specimens were subjected to freeze-thaw cycles.

This formulation can be employed to improve the design of subgrade subjected to freeze-thaw cycles under dynamic loading at studied conditions. Also, these findings well agree with the results concluded by Sadeghi and Beigi, (2014) [17].

6. Summary and conclusions

A number of the dynamic triaxial tests were conducted on unreinforced and fiber-reinforced soil subjected to closed-system freeze-thaw cycles. Also, to investigate the physical properties of fiber and soil

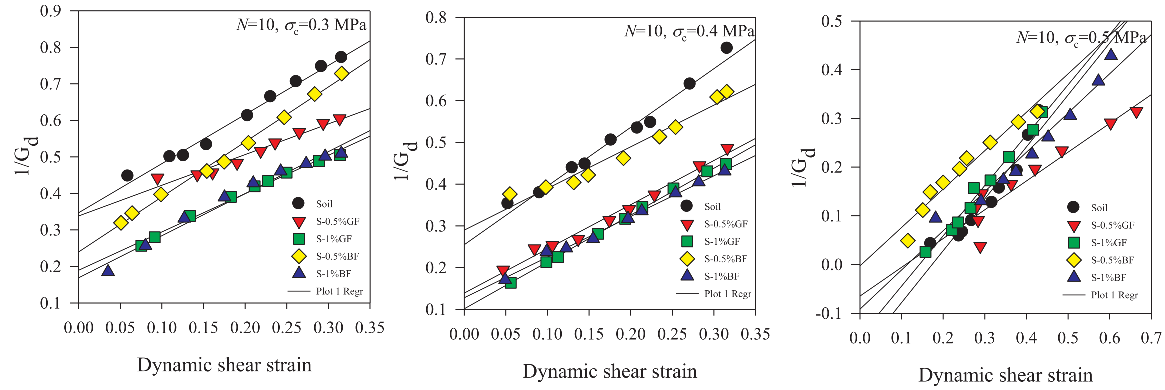

d. N=10, χ=0, 0.5 and 1%, σ_c=0.3, 0.4 and 0.5 MPa

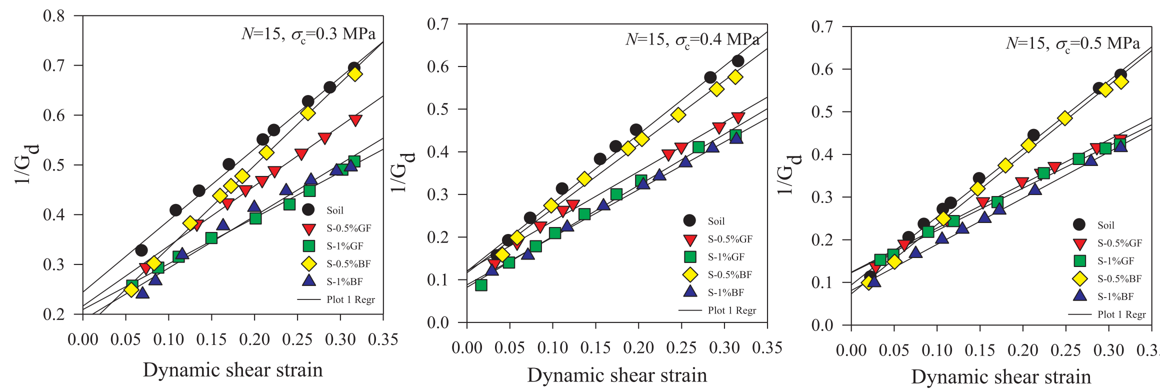

e. N=15, χ=0, 0.5 and 1%, σ_c=0.3, 0.4 and 0.5 MPa

Fig. 7. (*continued*)

Table 8
Calibrated parameters c_i and d_i.

c_o	c_1	c_2	c_3	c_4
1.575×10^{-5}	−0.054	−47.988	−9.859	−2.074
d_o	d_1	d_2	d_3	d_4
4.039×10^{-1}	−0.009	−41.192	−2.368	−0.425

Table 9
Impact functions on A and B for σ_c, N, w, χ_w.

Impact function	f_{χ}^{A}	f_{N}^{A}	f_{w}^{A}	$f_{\sigma c}^{A}$
$A = 1/G_d$	$(1+\chi)^{-47.99}$	$e^{-0.054} + e$	$w^{-9.86}$	$(\sigma_c/P_a)^{-2.07}P_a$
Impact function	f_{χ}^{B}	f_{N}^{B}	f_{w}^{B}	$f_{\sigma c}^{B}$
$B = 1/\sigma_{ult}$	$(1+\chi)^{-41.19}$	$e^{-0.009} + e$	$w^{-2.37}$	$(\sigma_c/P_a)^{-0.43}P_a$

mixtures subjected to freeze-thaw cycles, variations of water content and height were tested in an open system freeze-thaw cycles. The dynamic shear stress-strain curves, dynamic shear modulus and damping ratio versus dynamic shear strain were analyzed under different numbers of freeze-thaw cycles, volume fraction of fibers and different confining pressures. Then, the theoretical analytical formulations were used to determine dynamic shear modulus and dynamic shear stress–strain curves. The following conclusions are summarized as follows:

1. The most significant effects of freeze-thaw cycles on the physical properties including variations of water content and height was observed on the basalt fiber-reinforced soil. Also, the fibers influenced significantly mitigation on the frost heave. The 0.5% glass fiber-reinforced soil and the 0.5% basalt fiber-reinforced soil experienced the fifteen freeze-thaw cycles can be used to mitigate frost heave.
2. The dynamic axial stress increased with increments of fiber content, confining pressure and dynamic shear strain, but decreased after freeze-thaw cycles. Fiber-reinforced soil exhibited less reduction trend than unreinforced soil. The basalt fiber-reinforced soil can provide larger dynamic resistance than the glass fiber-reinforced soil because it has larger breaking strength and modulus of elasticity.
3. The Hardin-Drnevich model and the modified Kondner-Zelasko model were performed to define the relationships between the dynamic shear stress and dynamic shear strain. The results demonstrated that both models had a good agreement with experimental data. The remarkable relation was observed between dynamic shear stress and dynamic shear strain for all specimens.
4. The dynamic shear modulus of fiber-reinforced soil was greatly influenced by fiber content, confining pressure, freeze-thaw cycles and water content as well as shear strain. Dynamic shear modulus of fiber-reinforced soil increased with increments of fiber content, initial water content and confining pressure, and reduced with an increasing of the freeze-thaw cycles. Moreover, with addition of fiber content, damping ratio increased in all conditions.
5. The minimum magnitude of dynamic shear stress was observed after second and fifth freeze-thaw cycles, and then it increased with increasing of freeze-thaw cycles before it became stable at tenth cycle. It is recommended that the dynamic shear stress and dynamic shear modulus of the soil experienced five freeze-thaw cycles could be implemented to the engineering design in the seasonally frozen areas.
6. The theoretical analytical formulations were used to estimate the G

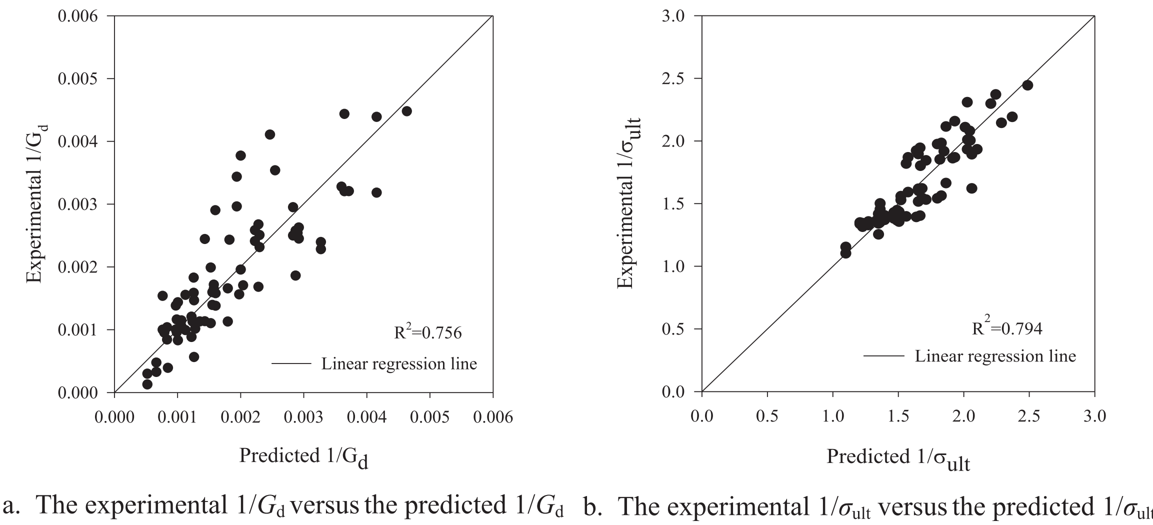

Fig. 8. Comparison of the model outputs predicted by nonlinear model and experimental data. a. The experimental $1/G_d$ versus the predicted $1/G_d$. b. The experimental $1/\sigma_{ult}$ versus the predicted $1/\sigma_{ult}$.

Table 10
The statistical data of $1/G_D$ and $1/\sigma_{ult}$.

$1/G_D$		$1/\sigma_{ult}$	
RSME	MRE (%)	RSME	MRE (%)
$6.53 \times 10^{-7} \sim 2.02 \times 10^{-4}$ **$R^2 = 0.756$**	$0.37 \sim 85.81$	$6.93 \times 10^{-5} \sim 7.20 \times 10^{-2}$ $R^2 = 0.794$	$0.04 \sim 27.68$

as a function of χ, N, w, and σ_c. To express the nonlinear behavior of the fiber-reinforced soil, ten constitutive coefficients of the formulation were calibrated by analyzing linear regression. The calibrated parameters showed that χ has a significant effect on $1/G_d$ and $1/\sigma_{ult}$ more than the other parameters. Moreover, when χ increases, increment of $1/G_d$ is larger than increment of $1/\sigma_{ult}$. Moreover, the formulation reflects the $1/G_D$ and $1/\sigma_{ult}$ for all soil specimens with $R^2 = 0.756$ and $R^2 = 0.794$, respectively.

Acknowledgments

This work was supported by the Foundation of the State Key Laboratory of Frozen Soil Engineering (05SS011101 SKLFSE201401), the National Natural Science Foundation of China (Grant Nos. 41171064 and 51378057) and the National Basic Research Program of China (973 Program, Grant No. 2012CB026104).

References

[1] Ghazavi M, Roustaei M. The influence of freeze-thaw cycles on the unconfined compressive strength of fiber-reinforced clay. Cold Reg Sci Technol 2010;61(2–3):125–31. http://dx.doi.org/10.1016/j.coldregions.2009.12.005.
[2] Roustaei M, Eslami A, Ghazavi M. Effects of freeze-thaw cycles on a fiber reinforced fine grained soil in relation to geotechnical parameters. Cold Reg Sci Technol 2015;120:127–37. http://dx.doi.org/10.1016/j.coldregions.2015.09.011.
[3] Zaimoglu AS. Freezing-thawing behavior of fine-grained soils reinforced with polypropylene fibers. Cold Reg Sci Technol 2010;60(1):63–5. http://dx.doi.org/10.1016/j.coldregions.2009.07.001.
[4] Botero E, Ossa A, Sherwell G, Ovando-Shelley E. Stress–strain behavior of a silty soil reinforced with polyethylene terephthalate (PET). Geotex Geomemb 2015;43(4):363–9. http://dx.doi.org/10.1016/j.geotexmem.2015.04.003.
[5] Tang CS, Wang DY, Shi B, Li J. Effect of wetting-drying cycles on profile mechanical behavior of soils with different initial conditions. Catena 2016;139:105–16. http://dx.doi.org/10.1016/j.catena.2015.12.015.
[6] Singh HP, Bagra M. Strength and stiffness response of Itanagar soil reinforced with jute fiber. Int J Innov Res Sci Eng Technol 2013;2(9):4358–67.
[7] Gullu H, Khudir A. Effect of freeze-thaw cycles on unconfined compressive strength of fine-grained soil treated with jute fiber, steel fiber and lime. Cold Reg Sci Technol 2014;106–107:55–65. http://dx.doi.org/10.1016/j.coldregions.2014.06.008.
[8] Noorzad R, Amini PF. Liquefaction resistance of Babolsar sand reinforced with randomly distributed fibers under cyclic loading. Soil Dyn Earthq Eng 2014;66:281–92. http://dx.doi.org/10.1016/j.soildyn.2014.07.011.
[9] Krishnaswamy NR, Isaac NT. Liquefaction potential of reinforced sand. Geotex Geomemb 1994;13(1):23–41. http://dx.doi.org/10.1016/0266-1144(94)90055-8.
[10] Krishnaswamy NR, Isaac NT. Liquefaction analysis of saturated reinforced granular soils. J Geotech Eng ASCE 1995;121(9):645–51. http://dx.doi.org/10.1061/(ASCE)0733-9410(1995)121:9(645).
[11] Vercueil D, Billet P, Cordary D. Study of the liquefaction resistance of a saturated sand reinforced with geosynthetics. Soil Dyn Earthq Eng 1997;16(7–8):417–25. http://dx.doi.org/10.1016/S0267-7261(97)00018-3.
[12] Ashmawy AK, Bourrdeau PL. Effect of geotextile reinforcement on the stress- strain and volumetric response of sand. In: Rowe RK, editor. 6th International Conference on Geosynthetics: Proceedings of the 6th International Conference on Geosynthetics; 1998 March 25–29; Georgia USA. Roseville, Minn.: Industrial Fabrics Association International; 1998: 1079–82.
[13] Ibraim E, Diambra A, Muir Wood D, Russell AR. Static liquefaction of fibre reinforced sand under monotonic loading. Geotex Geomemb 2010;28(4):374–85. http://dx.doi.org/10.1016/j.geotexmem.2009.12.001.
[14] Maheshwari BK, Singh HP, Saran S. Effects of reinforcement on liquefaction resistance of Solani sand. J Geotech Geoenviron Eng ASCE 2012;138(7):831–40. http://dx.doi.org/10.1061/(ASCE)GT.1943-5606.0000645.
[15] Shahnazari H, Ghiassian H, Noorzad A, Shafiee A, Tabarsa AR, Jamshidi R. Shear modulus of silty sand reinforced by carpet waste strips. J Seismol Earthq Eng 2009;11(3):133–42.
[16] Naeini SA, Gholampoor N. Cyclic behaviour of dry silty sand reinforced with a geotextile. Geotex Geomemb 2014;42(16):611–9. http://dx.doi.org/10.1016/j.geotexmem.2014.10.003.
[17] Sadeghi MM, Beigi FH. Dynamic behavior of reinforced clayey sand under cyclic loading. Geotex Geomemb 2014;42:564–72. http://dx.doi.org/10.1016/j.geotexmem.2014.07.0050266-1144.
[18] Kirar B, Maheshwari BK, Jakka RS. Dynamic properties of solani sand reinforced with coir fibers. Proceedings of the 15th World Conference on Earthquake Engineering; 2012 Sep 24–28; Lisbon, Portugal. Sociedade Portuguesa de Engenharia Sismica (SPES); 8771–8780; 2012.
[19] Nakhaei A, Marandi SM, Kermani SS, Bagheripour MH. Dynamic properties of granular soils mixed with granulated rubber. Soil Dyn Earthq Eng 2012;43:124–32. http://dx.doi.org/10.1016/j.soildyn.2012.07.026.
[20] Anastasiadis A, Senetakis K, Pitilakis K. Small-strain shear modulus and damping ratio of sand-rubber and gravel-rubber mixtures. Geotech Geol Eng 2011;30(2):363–82. http://dx.doi.org/10.1007/s10706-011-9473-2.
[21] Kanchi G, Neeraja V, Sivakumar Babu G. Effect of anisotropy of fibers on the stress-strain response of fiber-reinforced soil. Int J Geomech 2015;15(1):06014016. http://dx.doi.org/10.1061/(ASCE)GM.1943-5622.0000392.
[22] Yang X, Han J. Analytical model for resilient modulus and Permanent deformation of geosynthetic-reinforced unbound granular material. Geotex Geomemb 2013;139(9):1443–53. http://dx.doi.org/10.1061/(ASCE)GT.1943-5606.0000879.
[23] Li J, Ding DW. Nonlinear elastic behavior of fiber reinforced soil under cyclic loading. Soil Dyn Earthq Eng 2002;22(22):977–83. http://dx.doi.org/10.1016/S0267-7261(02)00122-7.
[24] Javadi A, Faramarzi A, Ahangar-Asr A. Analysis of behaviour of soils under cyclic loading using EPR-based finite element method. Finite Elem Anal Des 2012;58:53–65. http://dx.doi.org/10.1016/j.finel.2012.04.005.
[25] Bourrier F, Kneib F, Chareyre B, Fourcaud T. Discrete modeling of granular soils reinforcement by plant roots. Ecol Eng 2013;61:646–57. http://dx.doi.org/10.1016/j.ecoleng.2013.05.002.

[26] Khan M, Hossain M, Lozano N. Numerical study of slope stabilization using recycled plastic pin. In: Abu-Farsakh M, Yu X, Hoyos LR, editors. Geo-Congress 2014 Feb 23–26. Atlanta, Georgia: ASCE; 2014. p. 3092–101.

[27] Liu H, Won M. Stress dilatancy and reinforcement load of vertical reinforced soil composite: analytical method. J Eng Mech 2014;140(3):630–9. http://dx.doi.org/10.1061/(ASCE)EM.1943-7889.0000686.

[28] Amir-Faryar B, Sherif-Aggour M. Fiber-reinforcement optimization using a soil approach. In: Abu-Farsakh M, Yu X, Hoyos LR, editors. Geo-Congress 2014 Feb 23–26. Atlanta, Georgia: ASCE; 2014. p. 2523–32.

[29] Singha K. A short review on basalt fiber. Int J Text Sci 2012;1(4):19–28. http://dx.doi.org/10.5923/j.textile.20120104.02.

[30] Zimmie TF, Laplante CM, Bronson DL The effects of freezing and thawing on landfill covers and liners., Proceedings of the 3rd International Symposium on Cold Regions Heat Transfer. University of Alaska, Faibanks; 1991: 363–371.

[31] Wang D, Wei M, Yong-Hong N, Xiao-Xiao C, Zhi W. Effects of cyclic freezing and thawing on mechanical properties of Qinghai-Tibet clay. Cold Reg Sci Technol 2007;48:34–43. http://dx.doi.org/10.1016/j.coldregions.2006.09.008.

[32] Hardin BO, Drnevich VP. Shear modulus and damping in soils: measurement and parameter effects. ASCE: Soil Mech Found Division J 98. 1972; 1972. p. 603–24.

[33] Kondner RL, Zelasko JS. A hyperbolic stress–strain formulation of sands. Proceedings of the 2nd Pan-American Conference on Soil Mechanics and Foundation Engineering, Brazilian Association of Soil Mechanics, Sao Paulo, Brazil; (1) 289-324; 1963.

[34] Matasović N, Vucetic M. Cyclic characterization of liquefiable sands. J Geotech Eng 1993;119(11):1805–22. http://dx.doi.org/10.1061/(ASCE)0733-9410(1993)119:11(1805).

[35] Yi FF. Nonlinear cyclic characteristics of soils. Advances in analysis, modeling and design. In: Fratta DO, Puppala AJ, Muhunthan B, editors. GeoFlorida 2010: Proceedings of the GeoFlorida; 2010 Feb 20–24; Florida, USA 2010: 2601–2610.

[36] Maher MH, Woods RD. Dynamic response of sand reinforced with randomly distributed fibers. J Geotech Eng ASCE 1990;116(7):1116–31. http://dx.doi.org/10.1061/(ASCE)0733-9410(1990)116:7(1116).